7 A Perspective on Screened Coulomb Interactions from the constrained Random Phase Approximation

Jan M. Tomczak
Department of Physics, King's College London
Strand, London WC2R 2LS, UK

Contents

E. Pavarini, E. Koch, A. Lichtenstein, and D. Vollhardt (eds.)
Understanding Correlated Materials with DMFT
Modeling and Simulation Vol. 15
Forschungszentrum Jülich, 2025, ISBN 978-3-95806-813-1
http://www.cond-mat.de/events/correl25

1 Introduction

Electrons interact via the fundamental Coulomb force, which is long-ranged, strong, and universal. In a solid, the interaction an electron effectively experiences is often much weaker. This reduction arises from screening, the collective rearrangement of electrons in the material in response to a charge perturbation. As Anderson famously noted, "more is different" [1]: the collective behavior of many electrons cannot be reduced to pairwise interactions in isolation.
The constrained random phase approximation (cRPA), devised by Aryasetiawan *et al.* [2], provides a systematic framework for quantifying the screening in a materials-specific way. Crucially, cRPA allows one to disentangle screening processes arising from different energy scales. By separating screening contributions into low-energy (to be treated explicitly) and high-energy (to be integrated out) parts, cRPA yields effective interactions suited for use in low-energy settings, such as the Hubbard model. As such, this method has become a cornerstone in the realistic modeling of strongly correlated systems, bridging first-principles calculations and model Hamiltonians.
Several excellent reviews exist, in particular by Ferdi Aryasetiawan [3,4] from previous editions of the Jülich "Autumn School on Correlated Electrons". Highly recommended are also the reviews by Philipp Werner and Michele Casula [5] and by Silke Biermann [6].
The current notes require familiarity with elements of quantum-field theory for many-body systems (suitable books are, e.g., Refs. [7, 8]): The formalism of second quantization, (Matsubara) Greens functions, Wick's theorem, and Feynman rules will be employed.
The chapter is organized as follows. In Section 2 the random phase approximation (RPA) is introduced in the context of screening of the Coulomb interaction in a many-electron system. We will then derive simple results for the electron gas, the relevance of which will carry over to calculations of solids. We will briefly digress into discussing the GW approach, which will help us later to put into perspective how the effective interactions that cRPA provides typically are (or should be) used in higher-level many-body approaches.
Section 3 reviews the cRPA approach for the specific example of $SrVO_3$. We will discuss how an effective low-energy model for a subset of orbitals is obtained and compare its interaction to the bare as well as the fully screened interaction. Finally, we will contrast the level of material specificity contained in the cRPA interactions and how much of it is typically taken into account when solving the low-energy model.

2 The random phase approximation (RPA)

Broadly speaking, the random phase approximation[1] is a technique to approximately calculate susceptibilities χ of *interacting* systems. The principal advantage of the approach is that it only requires the explicit calculation of the system's free susceptibility, χ^0, i.e., the response in the absence of the inter-particle (Coulomb) interaction V. Nonetheless, the RPA suscepti-

[1]The RPA was originally introduced by Bohm and Pines in 1952. Details of the original derivation and the name the approach was given as a consequence is of little relevance today.

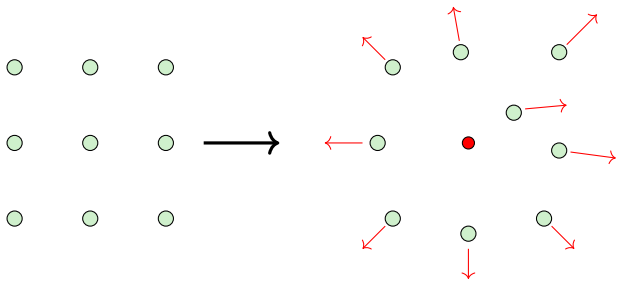

Fig. 1: *Coulomb repulsion in an electron gas* ○ ○ ○ *in presence of a (negative) test charge* ●. *The perturbation is mitigated (*screened*) as the system's density reacts to it.*

bility contains terms to all orders in the interaction strength by assembling an infinite series of Feynman diagrams from the building blocks χ^0 and V. Among others, the RPA can describe *collective* excitations (we will discuss the *plasmon*) and many-body renormalizations beyond Hartree-Fock (e.g., via the GW approach that we will sketch in Section 2.8).

2.1 Derivation of the RPA in the context of screening

The RPA is a fairly general approximation for susceptibilities associated with various degrees of freedom (e.g., spin, charge, or orbital in the context of solids). Here, we are interested in how the effect of a *fundamental* force between two particles (the Coulomb interaction) is modified if it is "simultaneously" experienced by a collection of many particles (electrons) that interact in a pairwise fashion from all to all. Imagine we subject our system of thus interacting electrons, which we describe with the Hamiltonian H, to an external perturbation V_t.

$$H_t = H + V_t \,. \tag{1}$$

We consider the case where $V_t = -\int d^3r\, \rho(\mathbf{r},t)\, V(\mathbf{r},t)$ is an explicitly time-dependent potential that describes the coupling of the system's charge density ρ to the (instantaneous) Coulomb interaction

$$V(\mathbf{r},t) = \frac{1}{4\pi\epsilon_0} \int d^3r' \frac{e^2}{|\mathbf{r}-\mathbf{r}'|}\, \rho_{\text{ext}}(\mathbf{r}')\, \delta(t) \tag{2}$$

arising from an *additional* external electron density $\rho_{\text{ext}}(\mathbf{r})$. Here, ϵ_0 is the permittivity of the vacuum. For example, $\rho_{\text{ext}}(\mathbf{r}') = \delta(\mathbf{r}')$ describes a single test charge at position $\mathbf{r}'$, see Fig. 1 for an illustration. The perturbation V_t will induce a change in the charge distribution of the original, unperturbed system. When Fourier-transforming to $\mathbf{q}$ and ω, this change is given by

$$\big\langle \delta\rho(\mathbf{q},\omega) \big\rangle = \big\langle \rho(\mathbf{q},\omega) \big\rangle - \big\langle \rho(\mathbf{q},\omega) \big\rangle_{V=0} = \frac{e^2}{\epsilon_0 q^2}\, \chi(\mathbf{q},\omega)\, \rho_{\text{ext}}(\mathbf{q},\omega) \tag{3}$$

where we used $\int d^3r \int d^3r' e^{i\mathbf{q}(\mathbf{r}-\mathbf{r}')}/|\mathbf{r}-\mathbf{r}'| = 4\pi/q^2$ for the Coulomb interaction. The response, or change in density, *screens* the perturbation: The extra charge density is accommodated by a rearrangement of the system's charge carriers, a process that effectively weakens the perturbation. The crucial idea now is to describe the external perturbation in a way that already accounts

(to an extent) for the system's reaction. The following Ansatz suggests itself

$$\big\langle \delta\rho(\mathbf{q},\omega)\big\rangle = \frac{e^2}{\epsilon_0 q^2}\,\tilde{\chi}(\mathbf{q},\omega)\big(\rho_{\text{ext}}(\mathbf{q},\omega) - \big\langle \delta\rho(\mathbf{q},\omega)\big\rangle\big). \tag{4}$$

In other words, we compute the response to a perturbation given by a modified "*screened*" external density, that we empirically choose as the original external density ρ_{ext}, *minus* the portion $\langle\delta\rho(\mathbf{q},\omega)\rangle$ of the system's charge that redistributes as a consequence of the initial "bare" perturbation. Since the perturbation has changed, also the response function is different from the one described by Eq. (3); we called it $\tilde{\chi}$. Note that (4) is a *self-consistent* equation: The anticipated change in density appears, both, on the left and on the right. Combining Eqs. (3) and (4), we obtain a relation between (a) the response χ to the *bare* perturbation and (b) the response $\tilde{\chi}$ to the *screened* perturbation

$$\chi(\mathbf{q},\omega) \;=\; \frac{\tilde{\chi}(\mathbf{q},\omega)}{1+\frac{e^2}{\epsilon_0 q^2}\tilde{\chi}(\mathbf{q},\omega)} \tag{5}$$

or, generalizing to an arbitrary interaction $V(\mathbf{q})$,

$$\chi(\mathbf{q},\omega) \;=\; \frac{\tilde{\chi}(\mathbf{q},\omega)}{1+V(\mathbf{q})\tilde{\chi}(\mathbf{q},\omega)}\,. \tag{6}$$

So far, we have not actually computed any susceptibility. We have only considered two settings that are, in principle, equivalent. The point now is that it stands to reason that *approximating* $\tilde{\chi}$ instead of χ is more promising, since the perturbation at its origin is, in a sense, weaker. That the perturbation is indeed effectively smaller can be seen as follows. We have

$$\big\langle \delta\rho(\mathbf{q},\omega)\big\rangle \overset{(4)}{=} V(\mathbf{q})\tilde{\chi}(\mathbf{q},\omega)\big(\rho_{\text{ext}}(\mathbf{q},\omega) - \big\langle \delta\rho(\mathbf{q},\omega)\big\rangle\big) \overset{(3)}{=} V(\mathbf{q})\chi(\mathbf{q},\omega)\rho_{\text{ext}}(\mathbf{q},\omega) \tag{7}$$

$$\equiv W(\mathbf{q},\omega)\tilde{\chi}(\mathbf{q},\omega)\rho_{\text{ext}}(\mathbf{q},\omega) \tag{8}$$

where we defined an effective interaction W, for which holds

$$W(\mathbf{q},\omega) = \frac{V(\mathbf{q})\chi(\mathbf{q},\omega)}{\tilde{\chi}(\mathbf{q},\omega)} \overset{(6)}{=} \frac{V(\mathbf{q})}{1+V(\mathbf{q})\tilde{\chi}(\mathbf{q},\omega)} = \epsilon^{-1}(\mathbf{q},\omega)V(\mathbf{q}) \leq V(\mathbf{q}) \tag{9}$$

where we introduced $\epsilon(\mathbf{q},\omega)$, the dielectric function, and the last inequality holds in the limit $(\mathbf{q}\to 0,\omega=0)$, since (as we will later show, see Eq. (47)) $\tilde{\chi}(\mathbf{q}\to 0,\omega=0)\geq 0$.
In the RPA, one performs the simplest possible approximation to the *screened* susceptibility: $\tilde{\chi} = \chi^0$. In other words, the screened response is approximated by the susceptibility of the *non-interacting* system. Consequently,

$$\chi^{\text{RPA}}(\mathbf{q},\omega) = \frac{\chi^0(\mathbf{q},\omega)}{1+V(\mathbf{q})\chi^0(\mathbf{q},\omega)} \tag{10}$$

$$W^{\text{RPA}}(\mathbf{q},\omega) = \frac{V(\mathbf{q})}{1+V(\mathbf{q})\chi^0(\mathbf{q},\omega)}\,. \tag{11}$$

While, now, the screened response that we will calculate is by construction independent of the inter-particle interaction, the RPA susceptibility depends on $V(\mathbf{q})$. However, this dependence

is merely *explicit*. Complicated two-particle expectation values for the interacting system are obviated, at the expense of including more complicated two-particle processes. As a consequence, we shall be able, in the following, to make use of Wick's theorem. This simplification allows the two-particle expectation, $\propto \langle c^\dagger\, cc^\dagger c\rangle$, to be factored into two one-particle expectation values, $\propto \langle c^\dagger c\rangle\langle c^\dagger c\rangle$, as for the purpose of the screened susceptibility we consider the electrons as non-interacting.[2]
For the following it will be useful to recall the geometric series, $\sum_{n=0}^{\infty} x^n = \frac{1}{1-x}$ for $|x| < 1$. Indeed, assuming convergence, we can rewrite the above RPA equations as a series expansion

$$\chi^{\mathrm{RPA}}(\mathbf{q},\omega) = \frac{\chi^0(\mathbf{q},\omega)}{1+V(\mathbf{q})\chi^0(\mathbf{q},\omega)} = \chi^0 + \chi^0(-V)\chi^0 + \dots \tag{12}$$

$$-W^{\mathrm{RPA}}(\mathbf{q},\omega) = \big[\underbrace{1+V(\mathbf{q})\chi^0(\mathbf{q},\omega)}_{\varepsilon(\mathbf{q},\omega)}\big]^{-1}(-V(\mathbf{q})) = \big[1+(-V)\chi^0+\dots\big](-V) \tag{13}$$

2.2 Diagrammatic representation

We will now make the connection to the description in terms of Feynman diagrams. In linear response theory (see, e.g., Refs [7, 8], the susceptibility that links a perturbation coupling to the system's charge density to its signatures in the same charge density can be written as

$$\chi^0(\mathbf{r},\mathbf{r}',t) = -\frac{1}{i\hbar}\Theta(t)\big\langle\big[\rho(\mathbf{r},t),\rho(\mathbf{r}',0)\big]\big\rangle_{H^0}. \tag{14}$$

Here, H^0 indicates that the free susceptibility is governed by an expectation value with respect to the non-interacting part of the system's Hamiltonian.
Making use of Wick's theorem, we can express χ^0 in terms of one-particle Green functions. For that, we first express the charge density in terms of field operators

$$\rho(\mathbf{r}) = \sum_\sigma \psi^\dagger_\sigma(\mathbf{r})\psi_\sigma(\mathbf{r}). \tag{15}$$

Here, $\psi^\dagger(\mathbf{r})$ creates an electron at a position $\mathbf{r}$ in continuum space. The connection with the perhaps more common formulation on a (discrete) lattice is made by introducing a basis set, e.g., in momentum-space $\{\varphi_{\mathbf{k}n}(\mathbf{r})\}$, whence

$$\psi_\sigma(\mathbf{r}) = \sum_{\mathbf{k}n} \varphi_{\mathbf{k}n}(\mathbf{r})c_{\mathbf{k}n\sigma}\,. \tag{16}$$

In the later parts of this section, we will study, for illustrative purposes, the charge response in the electron gas. We will therefore now assume a setting with a single band ($n = 1$) described

[2] Here, the RPA was derived through physical arguments for the density-density response. More generally, the RPA can be obtained through a truncation of the Green function's equation of motion (see, e.g., Ref. [7]): In the higher-order Green function that arises from the commutator with the interacting part of the Hamiltonian, one decouples the group of operators belonging, on the one hand, to the perturbation and, on the other hand, those from the particle-particle interaction in a mean-field fashion. Further, one approximates the arising expectation values by using only the non-interacting part of the Hamiltonian.

by plane waves, i.e., $\varphi_{\mathbf{k}}(\mathbf{r}) = \exp(i\mathbf{kr})$. While a more general formulation is of course possible (and used in practice), this setting will keep notation light. It follows that

$$\rho(\mathbf{r}) = \sum_{\sigma} \psi^{\dagger}_{\sigma}(\mathbf{r})\psi_{\sigma}(\mathbf{r}) = \sum_{\mathbf{k}\mathbf{k}'} c^{\dagger}_{\mathbf{k}\sigma} c_{\mathbf{k}'\sigma}\, e^{i(\mathbf{k}'-\mathbf{k})\mathbf{r}} = \sum_{\mathbf{k}\mathbf{q}\sigma} c^{\dagger}_{\mathbf{k}\sigma} c_{\mathbf{k}+\mathbf{q}\sigma}\, e^{i\mathbf{q}\mathbf{r}} \tag{17}$$

and writing χ in the Matsubara (imaginary time τ) formalism, we find

$$\chi^0(\mathbf{r},\mathbf{r}',\tau) = \sum_{\mathbf{k}\mathbf{q}\sigma}\sum_{\mathbf{k}'\mathbf{q}'\sigma'} \left\langle \mathcal{T}_\tau c^{\dagger}_{\mathbf{k}\sigma}(\tau) c_{\mathbf{k}+\mathbf{q}\sigma}(\tau) c^{\dagger}_{\mathbf{k}'\sigma'}(0) c_{\mathbf{k}'+\mathbf{q}'\sigma'}(0)\right\rangle_{H^0} e^{i\mathbf{q}\mathbf{r}} e^{i\mathbf{q}'\mathbf{r}'} \tag{18}$$

$$= \sum_{\mathbf{k}\mathbf{k}'\sigma\sigma' q} e^{i\mathbf{q}(\mathbf{r}-\mathbf{r}')} \left\langle \mathcal{T}_\tau c^{\dagger}_{\mathbf{k}\sigma}(\tau) c_{\mathbf{k}+\mathbf{q}\sigma}(\tau) c^{\dagger}_{\mathbf{k}'\sigma'}(0) c_{\mathbf{k}'-\mathbf{q}\sigma'}(0)\right\rangle_{H^0}. \tag{19}$$

Where we exploited momentum conservation, $\mathbf{k}+\mathbf{k}' = \mathbf{k}+\mathbf{q}+\mathbf{k}'+\mathbf{q}' \Leftrightarrow \mathbf{q}' = -\mathbf{q}$. Then, Wick's theorem tells us that there are two contractions that can be decoupled into pairs of Green functions

$$\chi^0(\mathbf{q},\tau) = \sum_{\mathbf{k}\mathbf{k}'\sigma\sigma'} \left\langle \mathcal{T}_\tau c^{\dagger}_{\mathbf{k}\sigma}(\tau) c_{\mathbf{k}+\mathbf{q}\sigma}(\tau) c^{\dagger}_{\mathbf{k}'\sigma'}(0) c_{\mathbf{k}'-\mathbf{q}\sigma'}(0)\right\rangle_{H^0} \tag{20}$$

$$= \sum_{\mathbf{k}\mathbf{k}'\sigma\sigma'} \underbrace{\left\langle \mathcal{T}_\tau c^{\dagger}_{\mathbf{k}\sigma}(\tau) c_{\mathbf{k}+\mathbf{q}\sigma}(\tau)\right\rangle}_{\delta_{\mathbf{q}\mathbf{0}}\, n_{\mathbf{k}\sigma}} \underbrace{\left\langle \mathcal{T}_\tau c^{\dagger}_{\mathbf{k}'\sigma'}(0) c_{\mathbf{k}'-\mathbf{q}\sigma'}(0)\right\rangle}_{\delta_{\mathbf{q}\mathbf{0}}\, n_{\mathbf{k}'\sigma'}} \tag{21}$$

$$+ \underbrace{\left\langle \mathcal{T}_\tau c^{\dagger}_{\mathbf{k}\sigma}(\tau) c_{\mathbf{k}'-\mathbf{q}\sigma'}(0)\right\rangle}_{G^0_{\mathbf{k}\,\sigma}(-\tau)} \underbrace{\left\langle \mathcal{T}_\tau c_{\mathbf{k}+\mathbf{q}\sigma}(\tau) c^{\dagger}_{\mathbf{k}'\sigma'}(0)\right\rangle}_{-G^0_{\mathbf{k}+\mathbf{q}}(\tau)\,\delta_{\mathbf{k}+\mathbf{q},\mathbf{k}'}\,\delta_{\sigma\sigma'}}$$

$$= \delta_{\mathbf{q}\mathbf{0}}\, n^2 - \sum_{\mathbf{k},\sigma} G^0_{\mathbf{k}\sigma}(-\tau)\, G^0_{\mathbf{k}+\mathbf{q}\sigma}(\tau) = \delta_{\mathbf{q}\mathbf{0}}\, n^2 + 0 \quad \underset{\mathbf{k},\,\sigma}{\overset{\mathbf{k}+\mathbf{q},\,\sigma}{\circlearrowright}}\ \tau\,. \tag{22}$$

The first term in Eq. (21) and following (where $n = \sum_{\mathbf{k}\sigma}\langle n_{\mathbf{k}\sigma}\rangle$) only contributes for $\mathbf{q} = 0$, i.e., it is uniform in space, $f(\mathbf{q}{=}0) = \int d^3r\, f(\mathbf{r})$. It is also τ-independent, i.e., static. Thus corresponding to a mere global shift of the origin of space, we will neglect this term. With only the bubble diagram remaining, and using Eq. (12), we see that the RPA consists of the following subset of 2-particle diagrams

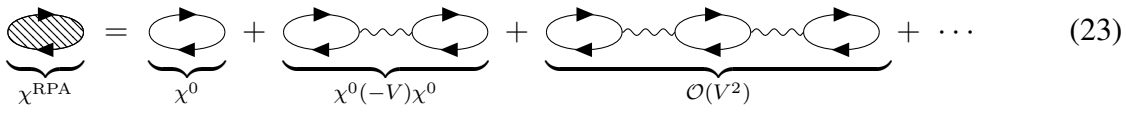

(23)

where the minus sign in front of V comes from the corresponding Feynman rule: one minus sign per power of the interaction. In turn, the screened interaction can be represented as

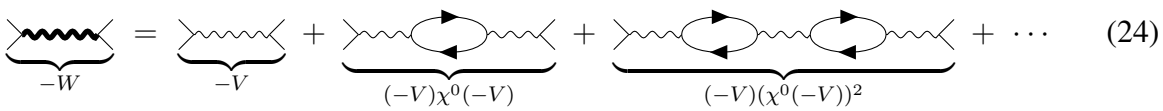

(24)

This (two-particle) series is similar to the (one-particle) Dyson equation for the one-particle Green function

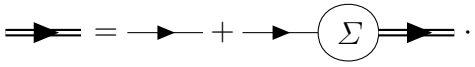

(25)

Indeed, in complete analogy, we can visualize Eq. (11) by

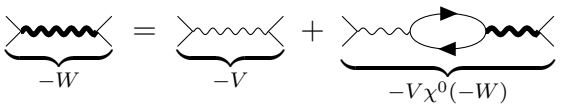

(26)

which is a so-called Bethe-Salpeter-equation (BSE), namely the one in the "particle-hole channel": Among the lines connecting V and W one points to the right and one to the left, corresponding to a particle propagating in time from 0 to τ and one propagating backwards in time, which we can alternatively identify as a hole propagating forward (cf. Eq. (22)).
The RPA is an approximation in that it contains only a subset of all possible two-particle diagrams. The general expression of the screened interaction, containing more or all diagrams, can be visualized by 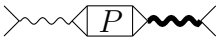 where P is a place-holder for all possible, so-called polarization diagrams[3]

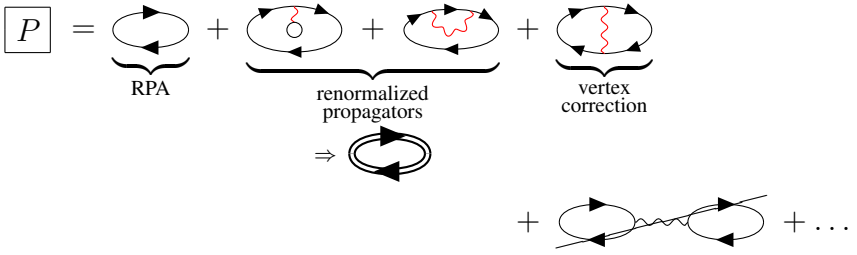

(27)

First, we note that the polarization only contains diagrams that are "V-irreducible". Indeed, diagrams that can be disconnected into two parts by cutting an interaction line (see, e.g., the stricken-out diagram above) are recursively generated in the BSE, Eq. (26), and have thus to be excluded in the polarization. This is in complete analogy to the irreducibility of the self-energy in terms of the propagator. There, the recursion in the Dyson equation generates diagrams that can be separated into two parts when cutting a Green function line. Second, the RPA is the lowest order approximation of the V-irreducible polarization. Higher order terms can be classified into two categories

1. Diagrams where individual Green function lines are dressed with self-energy insertions. These terms can be accounted for in so-called "bold" theories, where the free propagators G_0 (single line) are replaced with interacting Green functions (double line), see Eq. (27).

2. More complicated diagrams in which interactions couple different propagators. These terms are called "vertex corrections".

The RPA is non-perturbative in the sense that in the susceptibility, terms to all order in the interaction are generated (by virtue of the geometric series we do not have to compute them one-by-one). Still, as is evident from the above diagrams, there are contributions, again, at all orders, that are not included in the RPA. Therefore, the RPA is in practice still an approach best suited for weak coupling.

[3] In the cRPA and GW literature, instead of the charge-charge susceptibility χ, an object called the polarization $P = -\chi$ is used.

2.3 RPA for the electron-gas

2.3.1 Evaluation of χ^0

The evaluation of χ^0 is elementary in the Matsubara formalism

$$\chi^0(\mathbf{q},i\nu_n) = -2\sum_{\mathbf{k}}\sum_{i\omega_m}\frac{1}{\beta}G^0_{\mathbf{k}+\mathbf{q}}(i\omega_m+i\nu_n)\,G^0_{\mathbf{k}}(i\omega_m) \tag{28}$$

$$= -\frac{2}{\beta}\sum_{\mathbf{k}}\sum_{i\omega_m}\frac{1}{i\omega_m+i\nu_n-\varepsilon_{\mathbf{k}+\mathbf{q}}}\,\frac{1}{i\omega_m-\varepsilon_{\mathbf{k}}} \tag{29}$$

$$= -2\sum_{\mathbf{k}}\frac{1}{2\pi i}\oint dz\frac{f(z)}{(z+i\nu_n-\varepsilon_{\mathbf{k}+\mathbf{q}})(z-\varepsilon_{\mathbf{k}})} \tag{30}$$

$$= -2\sum_{\mathbf{k}}\frac{f(\varepsilon_{\mathbf{k}})-f(\varepsilon_{\mathbf{k}+\mathbf{q}})}{i\nu_n-(\varepsilon_{\mathbf{k}+\mathbf{q}}-\varepsilon_{\mathbf{k}})}, \tag{31}$$

where we used $\nu_n=\frac{2n\pi}{\beta}\rightarrow e^{i\beta\nu_n}=1\Rightarrow f(\varepsilon_{\mathbf{k}+\mathbf{q}}-i\nu)=f(\varepsilon_{\mathbf{k}+\mathbf{q}})$.Analytical continuation to real frequencies $i\nu\rightarrow\omega+i0^+$ leads to the (retarded) Lindhard function

$$\chi^0(\mathbf{q},\omega)=2\sum_{\mathbf{k}}\frac{f(\varepsilon_{\mathbf{k}+\mathbf{q}})-f(\varepsilon_{\mathbf{k}})}{\omega-(\varepsilon_{\mathbf{k}+\mathbf{q}}-\varepsilon_{\mathbf{k}})+i0^+}\,. \tag{32}$$

Quite generally, poles in propagators G or linear response susceptibilities χ describe eigenmodes of the system. Here, $\mathrm{Re}\,\chi^0(\mathbf{q},\omega)$ diverges for $\omega=\varepsilon_{\mathbf{k}+\mathbf{q}}-\varepsilon_{\mathbf{k}}>0$ if $\varepsilon_{\mathbf{k}}$ is an occupied and $\varepsilon_{\mathbf{k}+\mathbf{q}}$ an empty state, as dictated by the Fermi functions. One speaks of particle-hole excitations. These are illustrated in Fig. 2.

Had we allowed for the presence of multiple bands, n, we would have obtained a slightly more complicated Lindhard function of the form

$$\chi^0(\mathbf{q},\omega)=2\sum_{\mathbf{k}nn'}\Xi_{nn'}(\mathbf{k},\mathbf{q})\frac{f(\varepsilon_{\mathbf{k}+\mathbf{q}n'})-f(\varepsilon_{\mathbf{k}n})}{\omega-(\varepsilon_{\mathbf{k}+\mathbf{q}n'}-\varepsilon_{\mathbf{k}n})+i0^+} \tag{33}$$

where

$$\Xi_{nn'}(\mathbf{k},\mathbf{q})=\int d^3r\int\!d^3r'\,e^{-i\mathbf{q}(\mathbf{r}-\mathbf{r}')}\varphi^*_{\mathbf{k}n}(\mathbf{r})\varphi_{\mathbf{k}+\mathbf{q}n'}(\mathbf{r})\varphi^*_{\mathbf{k}+\mathbf{q}n'}(\mathbf{r}')\varphi_{\mathbf{k}n}(\mathbf{r}') \tag{34}$$

with the eigenfunctions $\varphi_{\mathbf{k}n}(\mathbf{r})=\langle\mathbf{r}|\mathbf{k}n\rangle$.

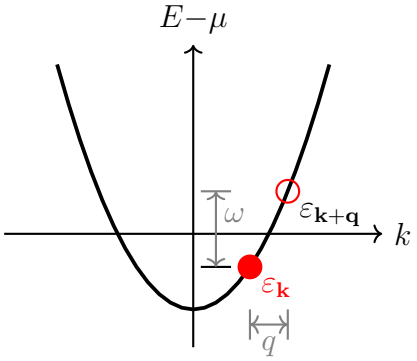

Fig. 2: *Particle-hole excitations. For an occupied state at $\varepsilon_{\mathbf{k}}$ and an unoccupied state at $\varepsilon_{\mathbf{k}+\mathbf{q}}$, the Lindhard function will have a pole for the indicated frequency $\omega>0$ and momentum $\mathbf{q}$.*

2.4 Excitations encoded in χ^{RPA}

What are the excitations encoded in the RPA susceptibility? For this, we perform in Fig. 3 a graphical analysis of

$$\chi^{\mathrm{RPA}}(\mathbf{q},\omega) = \frac{\chi^0(\mathbf{q},\omega)}{1+V(\mathbf{q})\chi^0(\mathbf{q},\omega)}\,. \tag{35}$$

at fixed momentum $\mathbf{q}$. The (real-part of the) RPA susceptibility diverges when the denominator cancels, i.e., $V(\mathbf{q})\chi^0(\mathbf{q},0) = -1$. First, we see that the poles of χ^0 translate into poles of χ^{RPA}. While individual poles are shifted, a dense continuum emerges in the thermodynamic limit that is shared between χ^0 and χ^{RPA}. This particle-hole continuum is confined by the possible values of $\varepsilon_{\mathbf{k}+\mathbf{q}}-\varepsilon_{\mathbf{k}}$: The *one-particle* spectrum available determines the energy/frequency range of these eigenmodes. The crucial observation now is that the $1/\omega$ decay in $\mathrm{Re}\,\chi^{RPA}$ causes an additional pole at $\omega = \omega_p$ *above* the one-particle continuum, whose existence hinges on the presence of the interaction V. This mode is called the *plasmon*. It corresponds to a quantum of *collective* plasma oscillations.

Classically, plasma oscillation can be understood as follows from electrodynamics: Consider a positively charged rigid and periodic ionic background, populated by negatively charged electrons. When electrons are displaced with respect to the ions, the Coulomb force tries to restore their equilibrium positions, acting as a "spring" causing the electrons to oscillate. Assuming an oscillating charge density $\rho(\omega) = \rho_0 \exp(-i\omega t)$, the continuity equation becomes $\nabla\cdot\mathbf{j} = -\partial\rho/\partial t = i\omega\rho(\omega)$. Combining with Ohm's law $\mathbf{j}(\omega) = \sigma(\omega)\mathbf{E}(\omega)$ and Gauss' law $\nabla\cdot\mathbf{E}(\omega) = \rho(\omega)/\epsilon_0$, one finds $i\omega\rho(\omega) = \sigma(\omega)\rho(\omega)/\epsilon_0$. For this equation to hold for an arbitrary $\rho(\omega)$ requires $\epsilon(\omega) \equiv 1 + i\sigma(\omega)/\epsilon_0\omega \stackrel{!}{=} 0$. According to Eq. (9), this is the same as demanding $1 + V(\mathbf{q})\chi^0(\mathbf{q},\omega) = 0$, which precisely holds for $\omega = \omega_p$, the plasmon! Above ω_p, absorption can no longer take place, and the system is transparent at those frequencies.

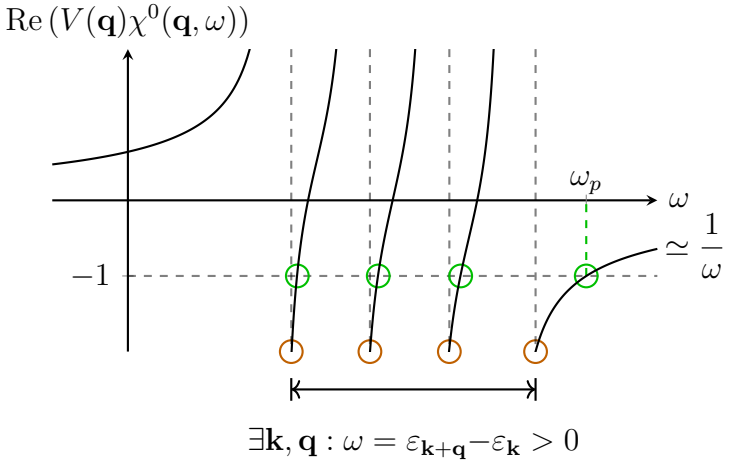

Fig. 3: *Eigenmodes encoded in the RPA susceptibility: The particle-hole continuum arising from accessible differences of one-particle energies,* $0 < \omega = \varepsilon_{\mathbf{k}+\mathbf{q}}-\varepsilon_{\mathbf{k}} < \omega_p$ *and the plasmon excitation in the electron gas.*

2.5 Properties of the plasmon

Consider $\chi(\mathbf{q},\omega)$ in the limit $\mathbf{q}\to 0$ at finite ω

$$\mathrm{Re}\,\chi^0(\mathbf{q},\omega) = -2\sum_{\mathbf{k}} \frac{f(\varepsilon_{\mathbf{k}}) - f(\varepsilon_{\mathbf{k}+\mathbf{q}})}{\omega - (\varepsilon_{\mathbf{k}+\mathbf{q}} - \varepsilon_{\mathbf{k}})} \tag{36}$$

$$= -2\sum_{\mathbf{k}} \left(\frac{f(\varepsilon_{\mathbf{k}})}{\omega - (\varepsilon_{\mathbf{k}+\mathbf{q}} - \varepsilon_{\mathbf{k}})} - \frac{f(\overbrace{\varepsilon_{-\mathbf{k}}}^{\varepsilon_{\mathbf{k}}})}{\omega - (\varepsilon_{-\mathbf{k}} - \varepsilon_{-\mathbf{k}-\mathbf{q}})} \right) \tag{37}$$

$$= -4\sum_{\mathbf{k}} f(\varepsilon_{\mathbf{k}}) \frac{(\varepsilon_{\mathbf{k}+\mathbf{q}} - \varepsilon_{\mathbf{k}})}{\omega^2 - (\varepsilon_{\mathbf{k}+\mathbf{q}} - \varepsilon_{\mathbf{k}})^2} \tag{38}$$

$$\overset{\mathbf{q}\to 0}{=} -\frac{2}{m\omega^2} \int \frac{d^3k}{(2\pi)^3}\, f(\varepsilon_{\mathbf{k}}) \big(\underbrace{2\,|\mathbf{k}|\,|\mathbf{q}|\cos\theta}_{=0 \text{ (angular integration)}} + \mathbf{q}^2 + \cdots \big) \tag{39}$$

$$= -\frac{n\mathbf{q}^2}{m\omega^2}, \tag{40}$$

where we made the replacement $k+q \to -k$ in the second term of Eq. (37), used the (even) symmetry of the dispersion $\varepsilon_{\mathbf{k}} = \hbar^2\mathbf{k}^2/2m = \varepsilon_{-\mathbf{k}}$,[4] and $n = 2\int \frac{d^3k}{(2\pi)^3} f(\varepsilon_{\mathbf{k}})$ is the number density of electrons. Neglecting $\mathrm{Im}\,\chi^{\mathrm{RPA}}$ in Eq. (10), this leads to

$$\chi^{\mathrm{RPA}}(\mathbf{q}\to 0,\omega) = \frac{-n\mathbf{q}^2/(m\omega^2)}{1 - V(\mathbf{q}) n\mathbf{q}^2/(m\omega^2)} = -\frac{n\mathbf{q}^2/m}{\omega^2 - \omega_p^2} \tag{41}$$

where, using the Coulomb interaction, $V(\mathbf{q}) = e^2/(\epsilon_0\mathbf{q}^2)$, we defined the plasma frequency

$$\omega_p = \sqrt{\frac{ne^2}{\epsilon_0 m}} > 0. \tag{42}$$

This limiting form of the RPA susceptibility clearly exposes the plasmon as an extra mode in the system. Typically, $\omega_p = \mathcal{O}(10\text{ eV})$. For example, in solid sodium, $\omega_p \approx 6$ eV [9].
Crucially, we note that the finite excitation energy for $q \to 0$ is intimately linked to the long-range nature of the Coulomb interaction (associated with the singularity of $V(q)$ at vanishing momentum). If the electrons were to interact via a short-range Yukawa interaction, $\frac{e^2}{\epsilon_0}\frac{1}{q^2+q_{\mathrm{TF}}^2}$ (with finite q_{TF}; see (46) below), (41) would yield a vanishing plasma frequency and a phenomenon known as "zero sound" emerges.[5]

[4] In the one-orbital case, $\varepsilon_{\mathbf{k}} = \varepsilon_{-\mathbf{k}}$ also holds (by virtue of Bloch's theorem) for dispersions on a lattice. For multi-orbital Hamiltonians, instead, inversion symmetry is required.

[5] The RPA procedure described here is very general. Applying the RPA formalism, e.g., to the spin-flip susceptibility of a ferromagnet, one finds a collective spin-excitation called the *magnon*, whose energy vanishes for $q \to 0$. In this case, the collective excitation is a so-called *Goldstone mode*: It is associated with the remaining all-up-or-all-down spin-flip freedom of the spontaneously broken spin-symmetry of the ferromagnetic state. Referring to the relativistic energy-momentum relation, $E = \sqrt{(pc)^2 + (m_0c^2)^2}$, zero sound and the magnon are called "massless" excitations ($m_0 = 0 \Rightarrow E \propto |p| \to 0\,(p \to 0)$), while the plasmon of the electron gas is a "massive" excitation.

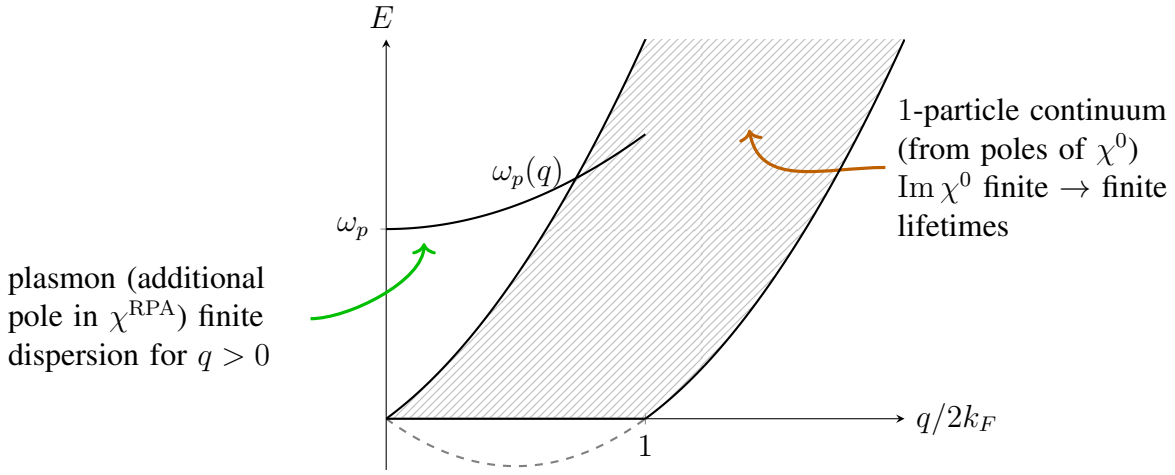

Fig. 4: *Excitation spectrum of the electron gas (in dimensions $d > 1$) within RPA. The shaded region delimits the particle-hole transitions between one-particle states, as already encoded in the free susceptibility. At small momentum q, there is an additional, collective mode: the plasmon. This excitation is a many-body effect. In fact, its existence requires the Coulomb repulsion between electrons.*

2.6 The excitation spectrum of the electron-gas within RPA

To put the *collective* plasmon mode into context to the particle-hole excitations described previously, we characterize their energy range. Transitions between one-particle states occur for poles in $\mathrm{Re}\,\chi^0$, i.e., for frequencies

$$\omega = \varepsilon_{\mathbf{k}+\mathbf{q}} - \varepsilon_{\mathbf{k}} = \frac{\hbar \mathbf{q}^2}{2m} + \frac{\hbar}{m} |\mathbf{k}|\,|\mathbf{q}| \cos\theta. \tag{43}$$

When we are in two or more dimensions, this yields a particle-hole continuum delimited by

$$\max(0, \frac{\hbar^2 q^2}{2m} - \frac{\hbar^2 k_F}{m} q) \leq \omega \leq \frac{\hbar^2 q^2}{2m} + \frac{\hbar^2 k_F}{m} q. \tag{44}$$

This range is visualized as a function of momentum q as the shaded region in Fig. 4. In particular, in the limit $q \rightarrow 0$, the particle-hole continuum vanishes (linearly). Consequently, for small momenta q, the "gapped" plasmon excitation lies far above the one-particle continuum.

2.7 Static screening (ω=0) in the long wavelength limit (q$\rightarrow$0)

We return to the motivation of these notes and study, how the response screens the Coulomb interaction within RPA. First, we specialize the Lindhard function to the static case (ω=0) in the long wavelength limit ($\mathbf{q}\rightarrow 0$). There,

$$\mathrm{Re}\,\chi^0(\mathbf{q}, \omega{=}0) = -2 \sum_{\mathbf{k}} \frac{f(\varepsilon_{\mathbf{k}}) - f(\varepsilon_{\mathbf{k}+\mathbf{q}})}{-(\varepsilon_{\mathbf{k}+\mathbf{q}} - \varepsilon_{\mathbf{k}})} \overset{\mathbf{q}\rightarrow 0}{=} 2 \sum_{\mathbf{k}} \left(-\frac{\partial f(\varepsilon_{\mathbf{k}})}{\partial \varepsilon_{\mathbf{k}}} \right) \overset{T=0}{=} N(0) \tag{45}$$

where we further assumed low temperatures and $N(0)$ is the value of the non-interacting system's density of states, $N(\varepsilon)=\sum_{\mathbf{k}\sigma}\delta(\varepsilon-\varepsilon_{\mathbf{k}})$, at the Fermi level. From this follows

$$W(|\mathbf{q}|\ll 1,\omega=0)=\frac{V(\mathbf{q})}{1+V(\mathbf{q})\chi^0(\mathbf{q},\omega=0)}=\frac{\frac{e^2}{\epsilon_0\mathbf{q}^2}}{1+\frac{e^2}{\epsilon_0\mathbf{q}^2}2N(0)}=\frac{e^2}{\epsilon_0}\frac{1}{\mathbf{q}^2+q_{\mathrm{TF}}^2}, \tag{46}$$

where $q_{\mathrm{TF}}=\sqrt{\frac{e^2}{\epsilon_0}N(0)}$ is the (inverse) Thomas-Fermi screening length. Fourier transforming this interaction to three-dimensional real-space, while assuming $W(|\mathbf{q}\ll 1,\omega=0)$ to be valid for all q, leads to the Yukawa potential

$$W(r)=\frac{e^2}{\epsilon_0\mathbf{r}}\,e^{-q_{\mathrm{TF}}|\mathbf{r}|}. \tag{47}$$

While the above derivation is approximate, this result provides important insights: In the presence of many particles interacting via the fundamental Coulomb force, the repulsion actually "felt" by the charge carriers is *screened*. Instead of a large and algebraically decaying interaction, $V(r)\propto 1/r$, the effective inter-electronic repulsion is reduced in magnitude and it becomes far more short-ranged. Note, in the present case of the electron gas, screening only occurs if the system is metallic ($N(0)>0$). Instead, in a solid, there are many bands or orbitals, both occupied and empty that contribute to χ^0, via inter-band transitions, see Eq. (33). Thus, while less efficient, screening also occurs in insulators.

The Yukawa form of the interaction can loosely be taken as a motivation of the Hubbard model. In its Hamiltonian the electron-electron interaction is assumed to be short-ranged to the extent that it is local.[6] Specifically, the Hubbard interaction takes the form $Un_{i\uparrow}n_{i\downarrow}$ with $n_{i\sigma}=c^\dagger_{i\sigma}c_{i\sigma}$: Only when electrons sit on the same lattice or atomic site i do they experience a repulsion U. The spin-structure of the interaction term is dictated by the Pauli principle because, in the absence of other quantum numbers (e.g., an orbital index), two electrons of the same spin cannot be present on the same site (at the same time).

2.8 The use of screened interactions: The GW approach

In Section 3 we will discuss how RPA-based techniques can be used to set up effective low-energy models from first principles. These models are typically cast into the form of a multi-orbital Hubbard Hamiltonian which is then solved with sophisticated many-body methods. However, there is great merit in directly using screened interactions W, of the kind that we just discussed. A popular and, at least formally, rather simple technique based on the screened interaction W is the GW approximation [10, 11]. Here, we will only provide two cartoon applications of this approach that will help us later to illustrate deficiencies in typical workflows for simulating correlated materials.

[6] It should be stressed that the Hubbard model is a lattice model. Hence, locality is to be understood in the sense of a Wannier orbital $\chi_{\mathbf{R}}(\mathbf{r})=\langle\mathbf{r}|\mathbf{R}\rangle$, i.e., as pertaining to a region in space surrounding a discrete position of an atomic site or unit-cell $\mathbf{R}$, instead of the point locality $\delta(\mathbf{r}-\mathbf{r}')$ in the continuum description of the electron gas.

As mentioned in the introduction, we cannot solve the full Hamiltonian that describes the solid we are interested in. One way to approximately simulate the system is the use of perturbation theory: We identify a parameter in the system, which, when set to zero, allows for a full solution of the problem. Then we perform a perturbative expansion in said parameter. At infinite order, we would describe the original problem exactly. The hope is, however, that if the parameter is small, a low-order expansion is sufficiently accurate.
Most frequently the interaction is considered as the perturbation to the exactly solvable non-interacting system. But which interaction to we perform our expansion in? The usual choice is the bare Coulomb interaction V. In that case, first-order perturbation theory amounts to the Hartree-Fock approximation. We could, however, make an expansion in terms of a screened interaction W. At infinite order, both expansions should yield identical results, but evaluations at finite order will differ. The argument for an expansion in W is, at least intuitively, straightforward: Screening reduces the interaction. The quantity we are expanding in is therefore a smaller parameter than the bare interaction—suggesting that a lower order in the expansion is sufficient than would be needed for the much larger bare interaction. Also, the RPA screening contains Feynman diagrams to all orders in the bare interaction, meaning that already a first-order expansion in W creates an infinite number of self-energy diagram. This first-order expansion is called the GW approximation. Diagrammatically, the GW self-energy is

$$\Sigma^{GW}_\sigma(\mathbf{k}, i\omega_n) = \quad = -\frac{1}{\beta}\sum_{i\omega_{n'},\mathbf{k}'} \underbrace{G^0(\mathbf{k}', i\omega_{n'})\, W(\mathbf{k}-\mathbf{k}', i\omega_n - i\omega_{n'})}_{\text{hence the name "}GW\text{"}} \tag{48}$$

$$= \quad + \quad + \quad + \ \ldots \tag{49}$$

We will now evaluate this GW diagram for two illustrative cases. Instead of computing the screened interaction, we will motivate typical forms of W for solid-state systems.

2.8.1 The non-local exchange self-energy

Let us first apply the GW approximation for the static, short-ranged (but still non-local!) Yukawa interaction from (46): $W(q) = \frac{e^2}{\epsilon_0}\frac{1}{q^2+q_{\mathrm{TF}}^2}$. For the sake of simplicity, we restrict the evaluation to one spatial dimension, set $T{=}0$, and assume a free-electron dispersion $\varepsilon_k = (\hbar k)^2/(2m)$ filled to the Fermi vector k_F. Then, an evaluation of the GW diagram is elementary, and yields

$$\Sigma(k) = (-1)^1(-1)^0 \sum_q \frac{1}{\beta}\sum_{n'} G^0(k{-}q, i\omega_{n'}) W(q) \tag{50}$$

$$= -\sum_q f(\varepsilon_{k-q}) W(q) \ = \ -\sum_{k'} \underbrace{f(\varepsilon_{k'})}_{\overset{T=0}{=}\theta(\varepsilon_{k_F}-\varepsilon_{k'})} W(k{-}k') \tag{51}$$

$$= -\frac{e^2}{\epsilon_0}\int_0^{k_F} dk' \, \frac{1}{(k{-}k')^2 + q_{\mathrm{TF}}^2} = \frac{e^2}{\epsilon_0 q_{\mathrm{TF}}}\left(\arctan\Big(\frac{k{-}k_F}{q_{\mathrm{TF}}}\Big) - \arctan\Big(\frac{k}{q_{\mathrm{TF}}}\Big)\right). \tag{52}$$

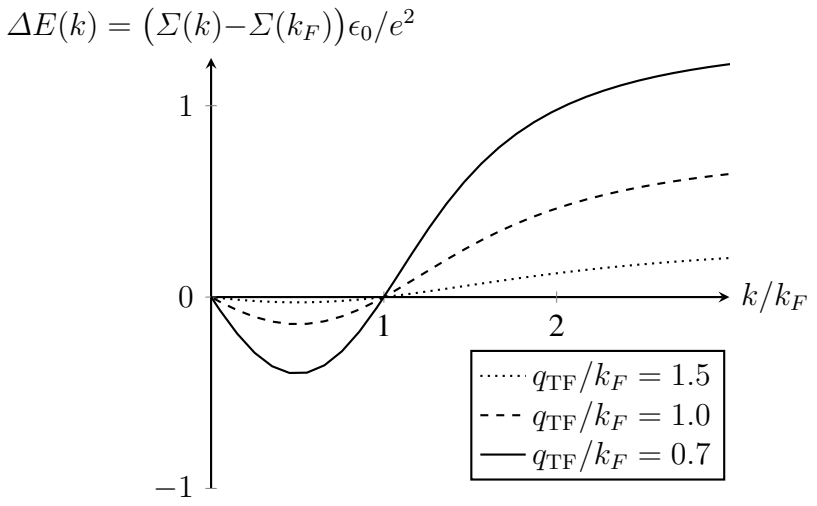

Fig. 5: *Momentum-dependence of the (toy-model's) exchange self-energy. Considering the renormalized energies, $\varepsilon_k \to \varepsilon_k + \Sigma(k)$, occupied states ($k < k_F$) are pushed down relatively to empty states ($k > k_F$), increasing the bandwidth or band-gap. Note: To conserve the particle number, the chemical potential has to adapt, e.g., in a coherent metal at $T{=}0$: $\mu \to \mu + \Sigma(k_F)$, which, here, we chose at the origin of energies.*

This self-energy, plotted in Figure 5, modifies the bare excitations ε_k in a way that is very different for occupied ($k/k_F < 1$) and for empty ($k/k_F > 1$) states. Indeed, in an effective dispersion, $\varepsilon_k \to \varepsilon_k + \Delta E(k)$, with $\Delta E(k) = \Sigma(k) - \Sigma(k_F)$, the former are pushed down, the latter are pushed upwards. Note that we added a chemical potential shift $\Sigma(k_F)$ to ΔE to assure conservation of particles (at $T{=}0$). This pulling away of states from the Fermi level enhances the bandwidth in a metal or the band-gap in a semiconductor.
This simplistic example highlights a crucial merit of the GW approximation, namely the non-local exchange contribution to the self-energy. Most notably, band gaps in semiconductors, such as Si or GaAs come out far too small in density-functional-based electronic structure methods. Through the mechanism illustrated here, the numerically more expensive GW approximation instead yields significantly larger and more accurate values for band gaps. This increase in kinetic energy (or band-gap) renders the system less correlated.

2.8.2 Self-energy from a dynamically screened interaction W

Screening is a dynamical process. Hence, the Lindhard function for χ^0, Eq. (32), the RPA susceptibility χ, Eq. (10), and the screened interaction W, Eq. (11), typically have a notable frequency dependence. A phenomenological form for the RPA screened interaction is[7]

$$W(\omega) = V + (V{-}U)\,\frac{\omega_p}{2}\left(\frac{1}{\omega{-}\omega_p + i0^+} - \frac{1}{\omega{+}\omega_p + i0^+}\right) = V + W_c(\omega) \tag{53}$$

[7]Note that the given $W(\omega)$ is the time-ordered version of the interaction, with which we could build Feynman diagrams with real frequencies. The relation to the retarded interaction $W^{\rm ret}(\omega)$ is $\mathrm{Re}\,W^{\rm ret}(\omega) = \mathrm{Re}\,W(\omega)$ and $\mathrm{Im}\,W^{ret}(\omega) = \mathrm{sgn}(\omega)\,\mathrm{Im}\,W(\omega)$.

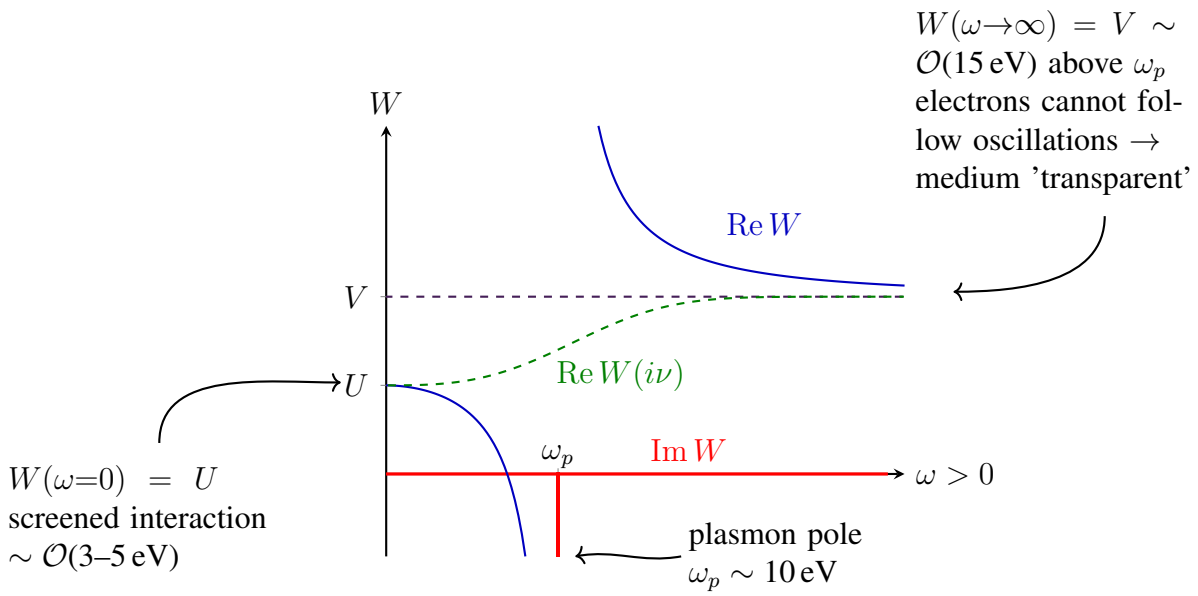

Fig. 6: *Phenomenological form of the frequency dependence of the RPA-screened interaction $W(\omega)$ on the real-axis. Also shown is the Matsubara counterpart $W(i\nu)$ which is purely real.*

that is illustrated in Figure 6: At large frequencies, screening is ineffective and the screened interaction approaches the bare Coulomb repulsion, $\text{Re}\,W(\omega{\to}\infty) \to V$. This can be understood from the electrodynamics point of view, already alluded to in Section 2.4: For frequencies above the plasma frequency ω_p, the system's electrons can no longer keep up with the fast pace of charge perturbations. The charges thus cease to mitigate the perturbation and the system becomes transparent. At the plasma frequency ω_p, which is a resonance (of the collective eigenmode) of the system, the interaction has a pole. Below ω_p, $\text{Re}\,W(\omega)$ is smaller than V and approaches a value $U < V$ in the static limit, as motivated by Thomas-Fermi theory above.

Comparing to the general form of the screened interaction in the RPA, Eq. (11), the expression above only accounts for the collective plasmon pole, not the electron-hole continuum arising from the Lindhard function. As such, it corresponds essentially to the $q \to 0$ limit for the electron gas discussed in Section 2.5. Further, in the case of a multi-band systems, inter-band transitions are neglected. Despite this limitation, Eq. (53) encodes well the overall shape of a screened interaction as computed from first principles, cf. Figures 6 and 9.
On the Matsubara axis, the dynamical part $W_c(\omega)$ of the interaction reads

$$W(i\nu) = \int d\omega \, \frac{-\frac{1}{\pi}\,\text{Im}\,W(\omega)}{i\nu - \omega} = g^2 \left(\frac{1}{i\nu - \omega_p} - \frac{1}{i\nu + \omega_p} \right) \tag{54}$$

with $g^2 = (V-U)\omega_p/2$.

Evaluation of the *GW* self-energy. Forgoing any complications of momentum-dependencies, let us assume a simplistic non-interacting electronic structure of a single level

$$H_0 = \varepsilon \sum_\sigma c_\sigma^\dagger c_\sigma \,. \tag{55}$$

Now, we have all the ingredients necessary to evaluate the GW diagram. We limit the calculation to the dynamical part of the interaction $W_c(\omega)$. Note also that, despite the name GW, the propagator in the diagram is the one of the non-interacting system, $G^0(i\omega_n)$.

$$\Sigma(i\omega_n) = -\frac{1}{\beta}\sum_{n'} G^0(i\omega_{n'})W_c(i\omega_n - i\omega_{n'}) \tag{56}$$

$$= -g^2\frac{1}{2\pi i}\oint dz \frac{f(z)}{z-\varepsilon}\left(\frac{1}{i\omega_n - z - \omega_p} - \frac{1}{i\omega_n - z + \omega_p}\right) \tag{57}$$

$$= -g^2\left(\frac{f(\varepsilon) - \overbrace{f(-\omega_p+i\omega_n)}^{-n_B(-\omega_p)\approx 1}}{i\omega_n - \varepsilon - \omega_p} - \frac{f(\varepsilon) + \overbrace{f(\omega_p+i\omega_n)}^{-n_B(+\omega_p)\approx 0}}{i\omega_n - \varepsilon + \omega_p}\right) \tag{58}$$

$$= -g^2\left(\frac{f(\varepsilon)-1}{i\omega_n - \varepsilon - \omega_p} - \frac{f(\varepsilon)}{i\omega_n - \varepsilon + \omega_p}\right). \tag{59}$$

Where we assumed $\omega_p \gg k_B T$. Let us further consider $\varepsilon \ll -1/\beta$, i.e., we require the state ε to be occupied, $f(\varepsilon) = 1$. Then the self-energy simplifies to

$$\Sigma(i\omega) = g^2\frac{1}{i\omega - \varepsilon + \omega_p} \overset{i\omega\to\omega+i0^+}{\longrightarrow} \Sigma(\omega) = g^2\frac{1}{\omega - \varepsilon + \omega_p + i0^+} \tag{60}$$

From this self-energy, we can obtain the excitation energies from the poles in the *interacting* Green function, $G(\omega) = [\omega - \varepsilon - \Sigma(\omega)]^{-1}$, i.e.,

$$\omega - \varepsilon - \mathrm{Re}\,\Sigma(\omega) \overset{!}{=} 0 \Leftrightarrow \omega - \varepsilon - \frac{g^2}{\omega - \varepsilon + \omega_p} = 0 \tag{61}$$

$$\rightarrow \omega_\pm = \varepsilon - \frac{\omega_p}{2} \pm \frac{\omega_p}{2}\sqrt{1 + \left(\frac{2g}{\omega_p}\right)^2} = \begin{cases} \varepsilon & + g^2/\omega_p \\ \varepsilon - \omega_p & - g^2/\omega_p \end{cases} + \mathcal{O}(g^4) \tag{62}$$

Hence, there are *two* peaks in the GW spectral function: ω_+ corresponds to the quasi-particle peak that shifts from its original position $\varepsilon < 0$ towards the Fermi level. In a solid with dispersive bands, this would correspond to a bandwidth narrowing. The other pole, ω_-, which for $g \ll \omega_p$ is at a distance of ω_p below the quasi-particle peak is the signature of the plasmon excitation encoded in $W(\omega)$.

The screened interaction thus causes a transfer of spectral weight from the quasi-particle peak to a plasmon satellite. We can estimate the transferred weight from the self-energy, akin to what is done in Fermi liquid theory. Indeed, assuming a form $\Sigma(\omega) = \Sigma(\omega{=}0) + (1 - \frac{1}{Z})\omega + \mathcal{O}(\omega^2)$ leads to a Green function $G(\omega) = \frac{1}{\omega - \varepsilon - \Sigma(\omega)} = \frac{Z}{\omega - Z(\varepsilon + \Sigma(0))} + G_{\mathrm{inc}}(\omega)$, where we have separated out incoherent contributions from higher energies into G_{inc}. Obtaining the quasi-particle weight Z from the derivative of the GW self-energy, we find[8]

$$Z = \left(1 - \frac{\partial\,\mathrm{Re}\,\Sigma}{\partial\omega}\right)^{-1}_{\omega=\varepsilon} = \left(1 + \frac{g^2}{(\omega_p - \varepsilon)^2}\right)^{-1} < 1 \tag{63}$$

[8] Alternatively, we could linearize around the bare level ε or the pole ω_+ instead of the Fermi level.

We see that spectral weight transfers, of magnitude $1-Z$, to the plasmon satellite that reduce the quasi-particle weight are large for states close to the Fermi level (small $|\varepsilon|$; $\varepsilon < 0$), large plasma frequency (ω_p; because $g^2 = (V-U)\omega_p/2$), and large screening effects (large $V-U$).[9]

The above two models illustrate the principal merits of the GW approximation:

1. the inclusion of momentum-dependent exchange contributions (that widen bandwidths) arising from non-local interactions

2. dynamical contributions (that cause bandwidth narrowing and satellite spectral features) originating from dynamical/retarded screening effects linked to the physics of plasmons.

3 The constrained RPA (cRPA)

For simulations of strongly correlated materials methodologies based on density-functional theory or the GW approximation are often insufficient. For example, the Mott transition and Kondo physics involve orbitals, typically from $3d$ and $4f$ shells, whose radial extent is small enough to reduce bandwidths to an extent that makes them comparable to the energy scale set by the Coulomb interaction. Then, interactions are no longer a perturbation to the almost-free electron picture and more sophisticated techniques have to be used. However, correlation effects are pronounced only for partially-filled orbitals that live close to the Fermi level. Further, higher-level many-body techniques commonly have an unfavorable scaling with the number of orbitals they can handle. Physics and methodological limitations thus suggest the use of effective setups that focus on a limited number of low-energy excitations. Identifying (or assuming) strong *local* interactions as dominating the physics allows for a further reduction of complexity, and, more often than not, the material problem is cast into the form of a multi-orbital Hubbard model. It is the workflow for this setting that we will describe in the following.

The overall goal is to devise a low-energy, few-orbital Hamiltonian that, when solved exactly, yields the same result for the degrees of freedom it contains as the exact solution of the initial full Hamiltonian of the solid [13]. Needless to say that exact solutions of neither the full nor the effective system are actually obtainable. The motivation is that for the model with less degrees of freedom, one could afford applying a more accurate methodology than would be possible for the initial Hamiltonian. A procedure that has become common practice is to seek the one-particle part of the desired low-energy Hamiltonian and its interaction terms *separately*.

[9] Clearly, the GW approximation is not exact. Thus, the question arises of how reliable it is. Incidentally, the electron-boson model, consisting of a spin-less level ε with the interaction $W(\omega)$ given, is exactly solvable [12]. The gist is that GW does well for the quasi-particle peak, $\omega_+^{\rm exact} = \varepsilon + g^2/\omega_p$ and $Z^{\rm exact} = e^{-(g/\omega_p)^2} = 1 - g^2/\omega_p^2 + g^4/(2\omega_p^4) + \ldots$, while the exact solution has infinitely many (instead of just one) plasmon satellites at $\omega_n^{\rm exact} = \varepsilon + g^2/\omega_p - n \times \omega_p$.

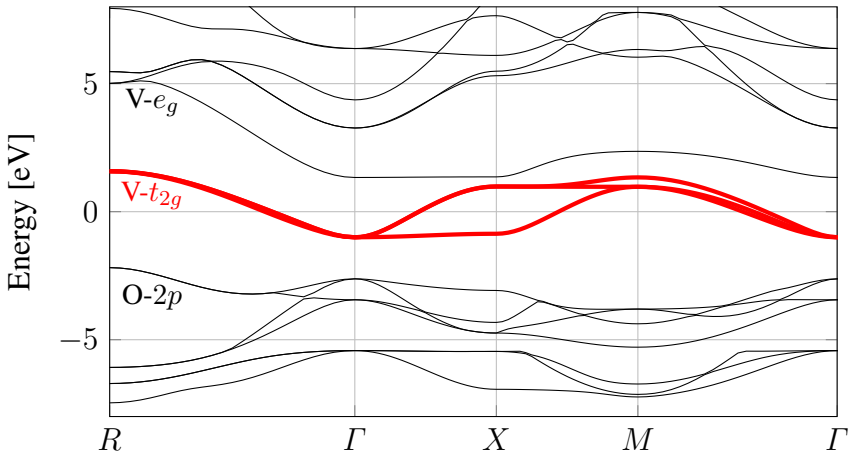

Fig. 7: *Band-structure of $SrVO_3$. DFT results (black) are overlaid with the bands of the maximally localized Wannier Hamiltonian for the vanadium t_{2g} orbitals (red). The Fermi level corresponds to the origin of energy.*

3.1 The one-particle part of the effective low-energy Hamiltonian

The starting point is a one-particle band-structure, e.g., obtained from density-functional theory-based approaches,[10] like the one shown in Figure 7 for the transition-metal oxide $SrVO_3$ or the sketch in Figure 8. We then identify a subset of bands (or an energy range) around the Fermi level that we believe to host the physics we wish to describe (e.g., the bands marked in red). We now interpret the dispersions of this target low-energy subspace as the one-particle ingredient to the interacting Hamiltonian that we seek. The assumption here is that DFT does not at all account for the physics that is to emerge from the interactions that we will supplement the dispersions with. Since the Kohn-Sham spectrum is a set of one-particle dispersions, the system's action is Gaussian and all undesired states can be integrated out. This procedure leads to a dynamical (or retarded) effective action for the small number of chosen states. A (static) Hamiltonian whose spectrum reproduces these low-energy dispersions can still be constructed through a linearization of this effective action, using or expanding on the idea of Löwdin downfolding [14]. A more elegant alternative is the use of (maximally localized) Wannier functions [15]. These functions, $\langle \mathbf{r}|\mathbf{R}L\rangle = \varphi_{\mathbf{R}L}(\mathbf{r})$, localized in a unit-cell R at the position of the atom hosting orbital L, are constructed from a subset of Bloch (or Kohn-Sham) states, $\psi_{\mathbf{k}n}(\mathbf{r})$ via a unitary transformation

$$\varphi_{\mathbf{R}L}(\mathbf{r}) = \frac{V}{2\pi}\int_{\mathrm{BZ}} d^3k\, e^{-i\mathbf{k}\mathbf{R}} \sum_n U^{(\mathbf{k})}_{nL}\psi_{\mathbf{k}n}(\mathbf{r}). \tag{64}$$

Essentially, Wannier orbitals are Fourier transforms of the Bloch eigenfunctions. However, (gauge) freedom allows for a unitary mixing instead of a mere 1-band (n) to 1-orbital (L) correspondence.[11] In maximally localized Wannier functions, this unitary ambiguity is used

[10] Although we remember that there is no actual justification for interpreting the auxiliary Kohn-Sham spectrum as the excitation energies of our system, empirically this works rather well.

[11] Complications may arise if the eliminated "high-energy" bands overlap or cross the low-energy sector. However, also for these situation a disentangling is possible, for details see Ref. [15].

to localize the Wannier function through minimization of the radial extent

$$\Omega = \sum_L \left(\langle \mathbf{R}L | \, \hat{\mathbf{R}}^2 \, | \mathbf{R}L \rangle - \left| \langle \mathbf{R}L | \, \hat{\mathbf{R}} \, | \mathbf{R}L \rangle \right|^2 \right), \tag{65}$$

where $\hat{\mathbf{R}}$ is the position operator. The Wannier orbitals are then used to construct the low-energy Hamiltonian, e.g., in real-space

$$H^0_{LL'}(\mathbf{R}) = \sum_{\mathbf{k}n} \varepsilon_{\mathbf{k}n} \, \langle \mathbf{0}L | \varphi_{\mathbf{k}n} \rangle \, \langle \varphi_{\mathbf{k}n} | \mathbf{R}L' \rangle = \sum_{\mathbf{k}} e^{-i\mathbf{k}\mathbf{R}} \left(U^{(\mathbf{k})^\dagger} \, \mathrm{diag}(\cdots \varepsilon_{\mathbf{k}n} \cdots) \, U^{(\mathbf{k})} \right)_{LL'} \tag{66}$$

As an example, we will discuss the transition-metal oxide $SrVO_3$. Strontium vanadate is a perfectly cubic perovskite in which Sr atoms sit at the corners of the cube, the V atom in the center and the O atoms at the face centers. The vanadium atom is thus surrounded by an oxygen octahedron, which causes a crystal-field that splits the V-$3d$ states into a low-lying t_{2g} triplet and a higher e_g doublet. With a nominal oxidation state of V^{4+}, the t_{2g} states are nominally filled with one electron. This partial filling places the t_{2g} states directly at the Fermi level, as can be seen in the DFT band-structure depicted in Figure 7. In the following, we shall be interested in constructing a low-energy model that solely comprises said t_{2g} states. If we were interested in the material's optical properties, say in the visual range, $\mathcal{O}$(1.6–3.3 eV), a setup that includes, at least, the O-$2p$ states and the V-e_g would be advisable.

Performing a Wannier projection onto the t_{2g} states provides us with the one-particle Hamiltonian, $H^0_{LL'}(\mathbf{k}) = \sum_{\mathbf{k}} \exp(i\mathbf{k}\mathbf{R}) H^0_{LL'}(\mathbf{R})$. Its eigenvalues trace the dispersion of the three t_{2g}-derived bands, as indicated by the red lines in Figure 7.

3.2 Interactions in the effective low-energy model

To compute the interacting part of the effective Hamiltonian, we need to account for the screening of all the states that we have eliminated. However, we do not want the *fully screened* interaction W that we have talked about before. We are seeking the *bare* interaction U of the effective Hamiltonian that describes the low-energy subspace. Indeed, maybe we want to perform perturbation theory in U or compute susceptibilities with beyond-RPA methods. So, the idea is to *constrain* the contributions to screening by eliminating all particle-hole transitions that occur within the target subspace, as detailed in (the caption of) Figure 8. This idea was pioneered by Ferdi Aryasetiawan *et al.* in Ref. [2][12] and is nowadays known as the *constrained random phase approximation (cRPA)*.

One thus separates the Lindhard function, Eq. (33), according to the start and end points of the particle-hole transitions into $\chi^0 = \chi^{0,\mathrm{high}} + \chi^{0,\mathrm{low}}$, where $\chi^{0,\mathrm{low}}$ contains all transitions that are confined to the low-energy subspace (red in Figure 8), and $\chi^{0,\mathrm{high}}$ all others. Then, we can define the *partially* screened interaction as

$$U(\mathbf{q},\omega) = \frac{V(\mathbf{q})}{1 + V(\mathbf{q}) \chi^{0,\mathrm{high}}(\mathbf{q},\omega)}, \tag{67}$$

[12] Worth mentioning are the some prequels [16, 17] and the sequel [18].

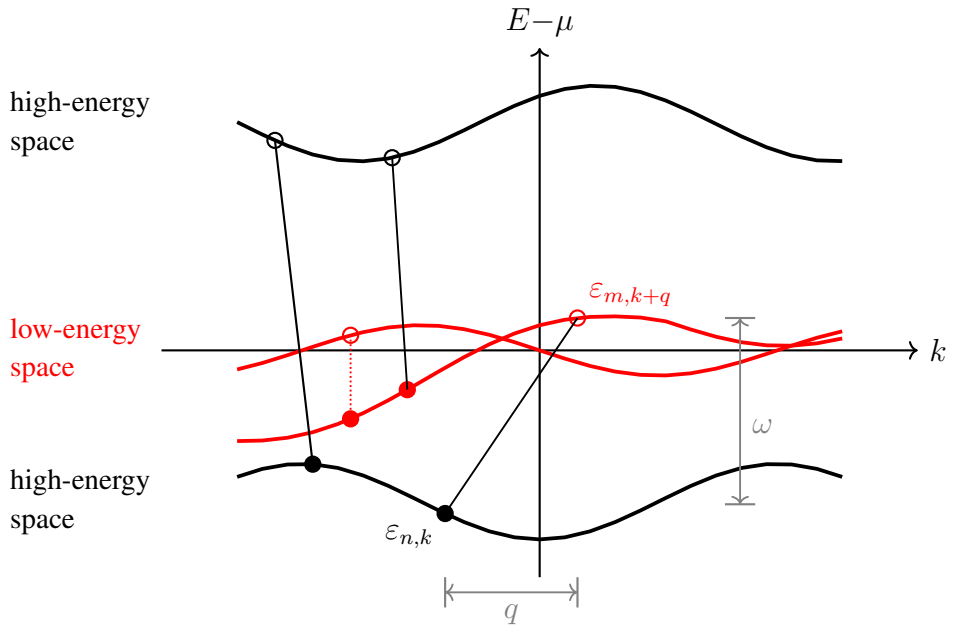

Fig. 8: *Contributions to the Lindhard function. The RPA employs as building block the free susceptibility, $\chi_0(\mathbf{q},\omega\geq 0)$, which sums up all possible transitions between (at $T=0$ occupied) states $\varepsilon_{n,k}$ and (empty) states $\varepsilon_{m,k+q}$. In cRPA, the band-structure is separated into high-energy (black) and low-energy (red) dispersions: We wish to eliminate the former, while the latter forms the one-particle ingredient to the effective Hamiltonian that we seek. To obtain an effective interaction for the low-energy subspace of orbital or bands, we constrain the contributing transitions to those that occur within the high-energy subspace, as well as transitions between the high-energy and the low-energy space. Examples for such transitions are indicated by solid black lines that connect an occupied state (solid circle) with an empty state (open circle). In other words, contributions to the screening that arise from transitions within the low-energy space are omitted. An example for such a transition is indicated by the red dotted line.*

and it is elementary to show that, when screening further, with $\chi^{0,\mathrm{low}}$, we recover the fully screened $W(\mathbf{q},\omega)=U(\mathbf{q},\omega)/(1+U(\mathbf{q},\omega)\chi^{0,\mathrm{low}}(\mathbf{q},\omega))$. To match up the interactions to the one-particle Hamiltonian, we transform the former into the Wannier basis [19],

$$V_{LL'}(\mathbf{R})=\langle L\mathbf{0},L'\mathbf{R}|\,V(\hat{\mathbf{R}})\,|L\mathbf{0},L'\mathbf{R}\rangle=e^2\int d^3r\int d^3r'\,\frac{|\varphi_{L\mathbf{0}}(\mathbf{r})|^2|\varphi_{L'\mathbf{R}}(\mathbf{r}')|^2}{|\mathbf{r}-\mathbf{r}'|} \tag{68}$$

$$U_{LL'}(\mathbf{R},\omega)=\int d^3r\int d^3r'\,|\varphi_{L\mathbf{0}}(\mathbf{r})|^2\left(\int d^3q\,e^{-i\mathbf{q}(\mathbf{r}-\mathbf{r}')}U(\mathbf{q},\omega)\right)|\varphi_{L'\mathbf{R}}(\mathbf{r}')|^2 \tag{69}$$

where, for simplicity, we limited ourselves to density-density type of interactions, $\propto n_{\mathbf{0}L}n_{\mathbf{R}L'}$. For $SrVO_3$, Figure 9 displays the resulting local ($\mathbf{R}$=0), intra-orbital ($L=L'\in\{1,2,3\}$; the t_{2g} are degenerate) interaction matrix elements in the Wannier basis: the bare interaction $V\in\mathbb{R}$, the partially screened cRPA Hubbard $U(\omega)$ and the fully screened RPA $W(\omega)$, where the latter two are complex at finite frequency. Looking at the static ($\omega=0$) limits, we see that screening with all electrons reduced the bare Coulomb interaction, $V=16.1\,\mathrm{eV}$, by more than one order of magnitude, to $W(0)=0.9\,\mathrm{eV}$. The effective interaction for the t_{2g} setup is still sizeable, $U(0)=3.5\,\mathrm{eV}$. From the inter-orbital matrix elements, we can further extract a Hund's rule coupling $J(\omega{=}0)=0.6\,\mathrm{eV}$.

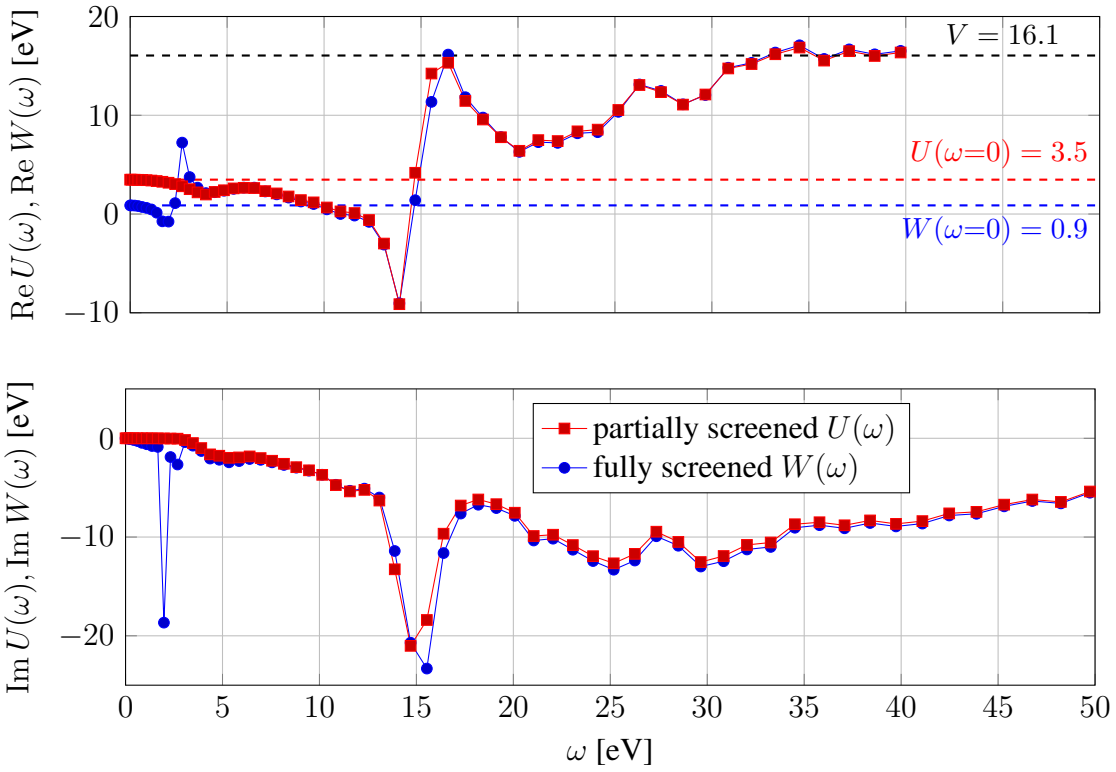

Fig. 9: *Local interactions of the t_{2g} orbitals of $SrVO_3$: the bare Coulomb interaction V (black dashed line; top panel), the RPA fully screened interaction $W(\omega)$ (blue circles; real (imaginary) part in top (bottom) panel); the cRPA partially screened Hubbard interaction $U(\omega)$ (red squares). All interactions refer to the on-site density-density intra-orbital matrix element in the t_{2g}-derived maximally localized Wannier basis. Increased screening contributions lead to the hierarchy $W(\omega{=}0) < U(\omega{=}0) < V$.*

The frequency dependence of U and W shares elements with the phenomenological plasmon-pole interaction shown in Figure 6: On top of a particle-hole background, we see in $U(\omega)$ [$W(\omega)$] one [two] plasmon resonances. The dominant one at $\omega \approx 15\,\mathrm{eV}$ corresponds to plasma oscillations that do not involve the V-$3d$ orbitals. This is corroborated by the fact that, electron-energy loss spectra (EELS: $\mathrm{Im}\,\epsilon^{-1}(\omega)$) of $SrTiO_3$ that nominally has one d-electron less, thus none at all, find a peak at the same frequency [20]. Instead, the low-energy plasma feature in $W(\omega{\approx}2\,\mathrm{eV})$ must derive from oscillations of the t_{2g} charge, as it is absent in $U(\omega)$ in which t_{2g} transitions are omitted.

This concludes our brief description of the setting up of the cRPA-based effective low-energy model, consisting of the one-particle Hamiltonian $H^0_{LL'}(\mathbf{k})$ and the interaction $U_{LL'}(\omega)$.

3.3 Caveats to how cRPA results are typically used

Here, we will not discuss critiques of the cRPA procedure outlined above, of which there are a few [21–23]. Rather, we will briefly point out deficiencies and skeletons in the closet in the way cRPA results are commonly used in, say, realistic dynamical mean-field theory (DFT+DMFT) calculations.

Dynamical interactions. Typically, DFT+DMFT simulations are performed with static interactions U instead of dynamical $U(\omega)$ ones. One might not have access to an *ab initio* computed $U(\omega)$. Also, impurity solvers that can work with retarded interactions are far less common and more expensive. A frequent procedure then is to simply use the cRPA interaction in the static limit $U(\omega{=}0)$, in the case of $SrVO_3$, $U(\omega{=}0) = 3.5\,\text{eV}$. However, it turns out that this interaction generates a mass enhancement far too small for simulations to match photoemission and specific-heat measurements. So, in various studies, the "solution" was to ramp up the interaction, in the case of $SrVO_3$, to $U = 5.0\,\text{eV}$ and mumble something about cRPA overestimating screening. Then, for $SrVO_3$, the effective mass enhancement, $m^*/m = Z^{-1} \approx 2$, comes out nicely indeed. Using the fictitiously enhanced U, half of the quasi-particle weight ($Z \approx 1/2$) is transferred to the *Hubbard bands* (cf. the chapters on DMFT in this book). But is this really the correct physics? In the GW model calculation in Section 2.8.2, we saw that a dynamical interaction (with a plasmon pole) caused a finite Z factor, Eq. (63), with spectral weight transferred to a *plasmon satellite*. Instead of artificially inflating the static U, could the plasmon peak or, generally, the frequency-dependence in $U(\omega)$ supply the missing mass-enhancement? Casula *et al.* [24], performing DFT+DMFT calculations with the *ab initio* $U(\omega)$ from Figure 9, answered this in the affirmative: They found the correct mass-enhancement as well has a lower Hubbard band in better agreement with experiment.

Non-local interactions. So, are DFT+DMFT calculations with $U(\omega)$ the ultimate answer? Reality turns out to be more complicated. While the occupied part of the spectrum (accessible from photoemission) comes out well for $SrVO_3$ using $U(\omega)$, an analysis [25] of the empty states suggests features are too close to the Fermi level. This time, the model calculation in Section 2.8.1 comes to the rescue: While screening reduces the range of the bare Coulomb interaction, the effective interaction experienced by the t_{2g} states is not strictly local (Hubbard-like). Then, a screened exchange contribution to the self-energy will widen the bandwidth, cf. Figure 5. With nominally 5/6 of the t_{2g} states being unoccupied, the anticipated increase in bandwidth will mostly be seen above the Fermi level. This insight is confirmed by GW [26] and so-called GW+DMFT calculations [27] for $SrVO_3$ [25, 28–33]. GW+DMFT combines the merits of both, GW (non-local exchange self-energy) and DMFT (dynamical local correlations).[13] From this vantage point, a provocative statement suggests itself [25]: The fact that DFT+DMFT calculations using $U(\omega{=}0)$ quite often do yield good results is owing to an error cancellation, the joint omission of mass renormalization from a dynamical $U(\omega)$ ($\rightarrow$ bandwidth narrowing) and non-local exchange contributions to the self-energy ($\rightarrow$ bandwidth widening).

One does not fit all. When applying many-body methods, such as DMFT, to materials, great care is taken to make the non-interacting part of the Hamiltonian as realistic as possible. Since correlations typically amplify any sort of polarization, it is indeed important to know whether,

[13] Note that a frequency-dependent local interaction can also be generated when treating non-local, say, nearest-neighbor interactions in the context of extended DMFT (EDMFT). For an instructive example using GW+(E)DMFT, see Ref. [34].

say, the t_{2g} orbitals in a transition-metal oxide are degenerate (as in metallic $SrVO_3$) or not (as in Mott-insulating $YTiO_3$) [35, 36]. Besides structural distortions in the bulk, also geometric constraints like a surface can lift degeneracies. For instance, in ultra-thin films of $SrVO_3$, this leads to a Mott-insulating state [37, 38] and a rich, orbital-physics driven phase diagram under doping [39].

The theoretical works cited in the preceding paragraph all used a static Hubbard U in their DMFT calculations. The additional caveat to mention here is that the *same* interaction was applied to all the (t_{2g}) orbitals. This is common practice. However, the Wannier functions, including their localization (Ω in Eq. (65)), will not be the same. Thus, already the matrix element of the bare interaction, V in Eq. (68), will differ from orbital to orbital. On top, the screening will be orbital-dependent as well. These differences in the interactions may enhance the degeneracy lifting in the non-interacting Hamiltonian. Or they could mitigate it.

The challenging truth is that correlated materials are extremely sensitive to minute details and trends are difficult to predict without explicit calculations. For instance, the dependence of the Hubbard U on external pressure or strain is highly-non-universal [40]: In the cuprate Bi_2CuO_4 pressure decreases U [41], while it goes up when straining La_2CuO_4 [42]. The fact that we are able to point this out is actually a sign of the field maturing. With methods such as the cRPA being available in more and more of the leading electronic structure packages, we are handed the tools for more realism and, hopefully, more quantitative predictions.

Acknowledgements

The author is indebted to Ferdi Aryasetiawan and Takashi Miyake who taught him the ropes of, among others, cRPA. Part of Section 2 derive from a chapter that the author wrote for the “Quantum field theory for many-body systems” course at TU Wien. Comments from my co-lecturers Karsten Held, Alessandro Toschi, and Anna Kauch are gratefully acknowledged. Special thanks go to Felix Höfenstock who in 2023 expertly turned my hand-written notes into LaTeX.

References

[1] P.W. Anderson, Science **177**, 393 (1972)

[2] F. Aryasetiawan, M. Imada, A. Georges, G. Kotliar, S. Biermann, and A.I. Lichtenstein, Phys. Rev. B **70**, 195104 (2004)

[3] F. Aryasetiawan, T. Miyake, and R. Sakuma in E. Pavarini, E. Koch, D. Vollhardt and A.I. Lichtenstein (eds.): *The LDA+DMFT approach to strongly correlated materials*, Modeling and Simulation, Vol. 1 (Forschungszentrum Jülich, 2011)

[4] F. Aryasetiawan in E. Pavarini, E. Koch, A. Lichtenstein, and D. Vollhardt (eds.): *DMFT: From Infinite Dimensions to Real Materials* Modeling and Simulation, Vol. 8 (Forschungszentrum Jülich, 2018)

[5] P. Werner and M. Casula, J. Phys.: Condens. Matter **28**, 383001 (2016)

[6] S. Biermann, J. Phys.: Condens. Matter **26**, 173202 (2014)

[7] W. Nolting: *Theoretical Physics 9: Fundamentals of Many-body Physics* (Springer, 2018)

[8] P. Coleman: *Introduction to Many-Body Physics* (Cambridge University Press, 2015)

[9] A. vom Felde, J. Sprösser-Prou, and J. Fink, Phys. Rev. B **40**, 10181 (1989)

[10] F. Aryasetiawan and O. Gunnarsson, **61**, 237 (1998)

[11] G. Onida, L. Reining, and A. Rubio, Rev. Mod. Phys. **74**, 601 (2002)

[12] D.C. Langreth, Phys. Rev. B **1**, 471 (1970)

[13] Y. Chang, E.G.C.P. van Loon, B. Eskridge, B. Busemeyer, M.A. Morales, C.E. Dreyer, A.J. Millis, S. Zhang, T.O. Wehling, L.K. Wagner, and M. Rösner, npj Comp. Mater. **10**, 129 (2024)

[14] P.-O. Löwdin, J. Chem. Phys. **19**, 1396 (1951)

[15] N. Marzari, A.A. Mostofi, J.R. Yates, I. Souza, and D. Vanderbilt, Rev. Mod. Phys. **84**, 1419 (2012)

[16] M. Springer and F. Aryasetiawan, Phys. Rev. B **57**, 4364 (1998)

[17] T. Kotani, J. Phys.: Condens. Matter **12**, 2413 (2000)

[18] F. Aryasetiawan, K. Karlsson, O. Jepsen, and U. Schönberger, Phys. Rev. B **74**, 125106 (2006)

[19] T. Miyake and F. Aryasetiawan, Phys. Rev. B **77**, 085122 (2008)

[20] S. Kohiki, M. Arai, H. Yoshikawa, S. Fukushima, M. Oku, and Y. Waseda, Phys. Rev. B **62**, 7964 (2000)

[21] Y. Nomura, M. Kaltak, K. Nakamura, C. Taranto, S. Sakai, A. Toschi, R. Arita, K. Held, G. Kresse, and M. Imada, Phys. Rev. B **86**, 085117 (2012)

[22] M. Kinza and C. Honerkamp, Phys. Rev. B **92**, 045113 (2015)

[23] E.G.C.P. van Loon, M. Rösner, M.I. Katsnelson, and T.O. Wehling, Phys. Rev. B **104**, 045134 (2021)

[24] M. Casula, A. Rubtsov, and S. Biermann, Phys. Rev. B **85**, 035115 (2012)

[25] J.M. Tomczak, M. Casula, T. Miyake, and S. Biermann, Phys. Rev. B **90**, 165138 (2014)

[26] T. Miyake, C. Martins, R. Sakuma, and F. Aryasetiawan, Phys. Rev. B **87**, 115110 (2013)

[27] S. Biermann, F. Aryasetiawan, and A. Georges, Phys. Rev. Lett. **90**, 086402 (2003)

[28] J.M. Tomczak, M. Casula, T. Miyake, F. Aryasetiawan, and S. Biermann, **100**, 67001 (2012)

[29] C. Taranto, M. Kaltak, N. Parragh, G. Sangiovanni, G. Kresse, A. Toschi, and K. Held, Phys. Rev. B **88**, 165119 (2013)

[30] R. Sakuma, P. Werner, and F. Aryasetiawan, Phys. Rev. B **88**, 235110 (2013)

[31] L. Boehnke, F. Nilsson, F. Aryasetiawan, and P. Werner, Phys. Rev. B **94**, 201106 (2016)

[32] J.M. Tomczak, P. Liu, A. Toschi, G. Kresse, and K. Held, Europ. Phys. J. Spec. Top. **226**, 2565 (2017)

[33] F. Nilsson, L. Boehnke, P. Werner, and F. Aryasetiawan, Phys. Rev. Mater. **1**, 043803 (2017)

[34] P. Hansmann, T. Ayral, L. Vaugier, P. Werner, and S. Biermann, Phys. Rev. Lett. **110**, 166401 (2013)

[35] E. Pavarini, S. Biermann, A. Poteryaev, A.I. Lichtenstein, A. Georges, and O.K. Andersen, Phys. Rev. Lett. **92**, 176403 (2004)

[36] E. Pavarini, A. Yamasaki, J. Nuss, and O.K. Andersen, New J. Phys. **7**, 188 (2005)

[37] K. Yoshimatsu, T. Okabe, H. Kumigashira, S. Okamoto, S. Aizaki, A. Fujimori, and M. Oshima, Phys. Rev. Lett. **104**, 147601 (2010)

[38] Z. Zhong, M. Wallerberger, J.M. Tomczak, C. Taranto, N. Parragh, A. Toschi, G. Sangiovanni, and K. Held, Phys. Rev. Lett. **114**, 246401 (2015)

[39] M. Pickem, J. Kaufmann, K. Held, and J.M. Tomczak, Phys. Rev. B **104**, 024307 (2021)

[40] J.M. Tomczak, T. Miyake, R. Sakuma, and F. Aryasetiawan, **79**, 235133 (2009)

[41] D. Di Sante, A. Hausoel, P. Barone, J.M. Tomczak, G. Sangiovanni, and R. Thomale, Phys. Rev. B **96**, 121106 (2017)

[42] O. Ivashko, M. Horio, W. Wan, N.B. Christensen, D.E. McNally, E. Paris, Y. Tseng, N.E. Shaik, H.M. Rønnow, H.I. Wei, C. Adamo, C. Lichtensteiger, M. Gibert, M.R. Beasley, K.M. Shen, J.M. Tomczak, T. Schmitt, and J. Chang, Nat. Commun. **10**, 786 (2019)